Photochemistry of NO Chemisorbed on TiO_2(110) and TiO_2 Powders

C. N. Rusu and J. T. Yates, Jr.*

University of Pittsburgh, Department of Chemistry, Surface Science Center, Pittsburgh, Pennsylvania 15260

Received: June 30, 1999; In Final Form: December 20, 1999

The photodecomposition of chemisorbed NO has been studied using ultraviolet radiation of (3.96 ± 0.07) eV. Both the TiO_2 (110) single-crystal substrate and high area compressed TiO_2 powders have been investigated. A primary photoproduct is N_2O gas, which desorbs immediately upon irradiation of the TiO_2 (110) surface. Following this process, the photoproduction of NO gas is observed to reach a maximum rate and then to decline. The cross section for the initial photodepletion of NO is about 1×10^{-15} cm^2, corresponding to a quantum efficiency near unity. In contrast, the quantum efficiencies of gas-phase N_2O and NO photoproduction from chemisorbed NO on TiO_2 are only in the range $10^{-2}-10^{-4}$, indicating that NO photodecomposition primarily yields an intermediate photoproduct (N_2O) which is captured on the crystal surface at 118 K. Studies of the infrared spectral behavior of NO on powdered and compressed high area TiO_2 powders during photolysis confirm that much of the N_2O photoproduct is retained on the surface. Furthermore, the infrared studies indicate that the penetration of ultraviolet light into the powder occurs to a depth of order 0.003 cm, which is very large compared to the light attenuation length known for individual TiO_2 crystals (200 Å). This effect is thought to be due to light transport effects at the particle boundaries in the compressed powder, and this effect therefore is favorable for photoprocesses using powders. Evidence for sub-bandgap excitation of chemisorbed NO, leading to N_2O production is presented.

I. Introduction

Among the most important atmospheric pollutant gases emitted by combustion are the nitrogen oxides (NO_x). The major emission product is nitric oxide (NO). The photochemical destruction of NO molecules adsorbed on TiO_2 is a viable method for the removal of this molecule from gaseous emissions. Since TiO_2 is a photocatalyst which may be activated by the UV portion of the solar spectrum, NO abatement by solar-driven photocatalysis on TiO_2 surfaces is feasible. This paper is concerned with fundamental aspects of NO photodecomposition on TiO_2 surfaces and the measurement of the efficiency of this desirable photoreaction.

For the control of combustion processes it is important to diminish the concentration of nitric oxide. In this connection, the selective catalytic reduction (SCR) of NO with NH_3,[1,2] with hydrocarbons[3] [called HC−SCR], or with oxygenated hydrocarbons using zeolite-based catalysts[2,4,5] or alumina[6−8] or titania based oxides[3] and supported noble metals[9] have been reported. The formation of surface inorganic species such as nitrate $-NO_3^-$, nitro $-NO_2$, and nitrite $-NO_2^-$ were observed.

Another approach for NO_x control is selective adsorption. The NO adsorption rate should be high and the process reversible in order to reopen the adsorption sites. Yang et al.[10] demonstrated a high adsorption capability of TiO_2 for NO. It was found that sulfonation of Degussa TiO_2 slightly decreased the NO adsorption capacity, but significantly increased the reversibility of the NO adsorption/desorption process.

The electronic structure of NO is very similar to that of the CO. The main difference lies in the fact that NO has one electron in the antibonding $2\pi^*$ orbital whereas this orbital is empty in the case of CO. This lowers the dissociation energy from 1070 kJ/mol (CO) to 678 kJ/mol (NO). Thus, in gas phase, the tendency for NO to dissociate is more favorable than for CO. The coordination chemistry of the NO molecule is complicated because of this extra electron in the antibonding $2\pi^*$ orbital. The NO molecule exhibits both electron donor and electron acceptor behavior in its coordination chemistry.

The thermally activated surface behavior of NO on TiO_2 has been studied and forms a basis for understanding the photochemistry of NO. Recent studies[11] have shown that NO adsorption on defective TiO_2(110) produces N_2O by a thermally activated process. The N_2O reduction product was observed in temperature programed desorption (TPD) studies to desorb with rate maxima at 169 and 250 K. The intensity of the lower temperature N_2O desorption feature was proportional to the coverage of defect sites created and was caused by the decomposition of NO at the $Ti^{3+}(3d^1)$ defect sites created in the annealing process.[12,13] These defect sites were completely removed upon oxidation by adsorbed NO. Boccuzzi et al.[14−17] studied NO adsorbed on powdered TiO_2 using FTIR measurements. From the restoration of the transparency of the reduced TiO_2 by NO to almost the same value as for the oxidized sample, the authors concluded that dissociative chemisorption of the NO occurs with loss of the electron trapped in the $Ti^{3+}(3d^1)$ orbital followed by NO conversion to N_2O. Thermal desorption measurements made by Pande et al.[18] observed both NO and N_2O desorption from NO adsorbed on reduced TiO_2. Increasing the defect density on the surface led to an increase in the NO reduction yield to N_2O and N_2. On the 1073 K reduced TiO_2, only N_2 and N_2O were produced by thermal excitation. As a consequence of the IR study of NO adsorption on TiO_2(anatase), Dines and al.[19] proposed the formation of bridging and bidentate nitrato adsorbed species. The formation of the bidentate nitrato species from NO, in comparison with NO_2 that gave only monodentate nitrato species, is probably due to the NO interaction with two surface oxygen atoms to form nitrato species.

10.1021/jp992239b CCC: $19.00
Published on Web 02/04/2000

Only a few papers have been published concerning the surface photochemistry of NO on TiO_2, although the photochemistry of many molecules on TiO_2 is well documented as shown in a recent review.[20] The photochemistry over an n-type semiconductor, such as TiO_2, is based on the fact that an electron is excited from the valence band to the conduction band when TiO_2 is irradiated with photons whose energy is equal to or larger than the band gap. Under these conditions, the charges are separated and the semiconductor can behave as a photocatalyst. The electrical neutrality of the substrate is maintained either by direct electron−hole pair recombination or by equivalent rates for the holes reacting with oxidizable species and the electrons being captured by reducible species.

Photoreactions of NO have been reported for a large number of surfaces, especially metals.[21] To the best of our knowledge, the study of NO photochemistry on single-crystal $TiO_2(110)$ has not been reported. Pichat et al.[22] studied the modification of the photoconductivity of TiO_2 powder as NO adsorption takes place. An inverse dependence of the TiO_2 photoconductivity on the NO pressure was interpreted as indicating that each NO molecule is chemisorbed by capturing one semiconductor bound electron. Courbon and Pichat[23] have investigated the photocatalytic decomposition of NO on prereduced and preoxidized TiO_2 (anatase) powder, and they found that the powdered TiO_2 photocatalyst decomposes NO, at room temperature, into N_2O molecules and not into N_2 and O_2. T. Ibusuki and K. Takeuchi[24] showed that NO is converted under UV irradiation to nitric acid (HNO_3) in the presence of water, but some NO is also oxidized to nitrogen dioxide (NO_2) which was then adsorbed by activated carbon which had been mixed with the TiO_2. Thus, they conclude that a mixture of TiO_2 and activated carbon is an excellent photoassisted catalyst for the removal of low concentrations of NO_x from air. They found that the addition of 1−3 wt % Fe_2O_3 could markedly increase the catalytic activity. Schaper and Hesse[25] found also that NO photodecomposes on powdered TiO_2 under UV irradiation forming N_2O; O_2 product was not observed. They found that the TiO_2 catalyst is poisoned by oxygen and cannot be regenerated by annealing the crystal at 353 K. Yamashita et al.[26] found that titanium dioxide anchored in Y-zeolite cavities exhibits an interesting photocatalytic activity for NO decomposition at 275 K. The formation of N_2 in the photocatalytic decomposition of NO was achieved with the TiO_2/Y-zeolite catalyst, having highly dispersed isolated tetrahedrally coordinated Ti^{4+} sites coordinated to oxide anions in the zeolite, while the formation of N_2O in the photocatalytic decomposition of NO was found to proceed on bulk TiO_2 catalysts and on the TiO_2/Y-zeolite catalysts involving aggregated octahedral coordinated Ti^{4+} species.

The work reported here involves studies of NO photochemistry on $TiO_2(110)$, containing surface anion vacancy sites. Measurements of the cross section for photochemical decomposition of NO are reported. In addition, studies on powdered TiO_2 surfaces have provided insight into the nature of the surface species consumed and produced upon NO photolysis, as well as information on the penetration depth for UV radiation in compressed powdered TiO_2.

II. Experimental Methods

A. NO Photochemistry on $TiO_2(110)$. This work on the photodecomposition of chemisorbed NO has been carried out on a $TiO_2(110)$ single crystal and also on a high area powdered TiO_2 substrate. In both cases, to eliminate thermal excitation processes, thereby permitting the study of pure photoexcitation processes, the NO/TiO_2 surfaces were kept at temperatures near 110 K.

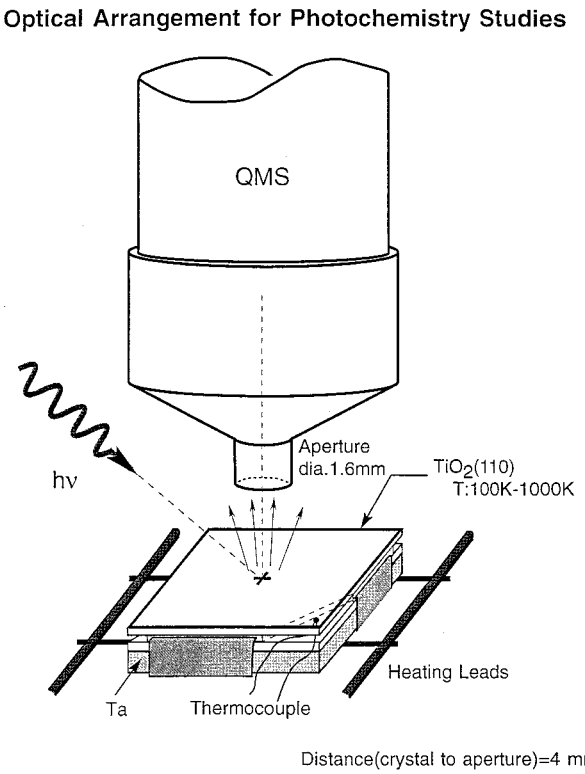

Figure 1. Optical arrangement for photochemistry studies on a $TiO_2(110)$ single crystal. The relative position of the QMS, the crystal, and the UV beam are shown.

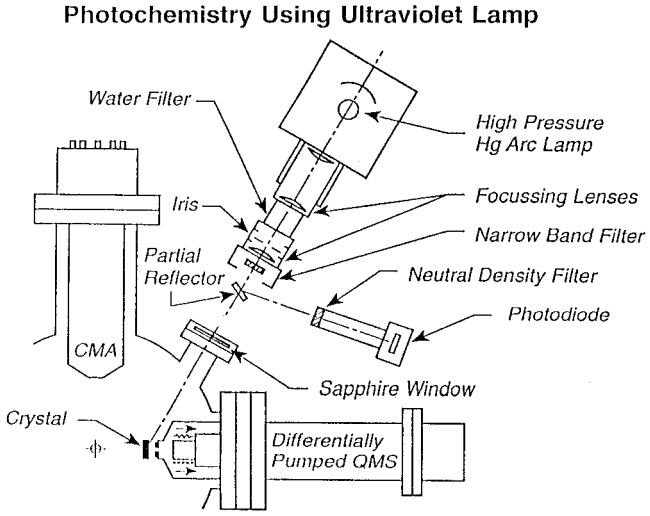

Figure 2. Top view of the UHV chamber, illustrating the arrangement of the single crystal, UV lamp and optical bench, and surface probes.

Studies of the photodecomposition and photodesorption of NO on TiO_2 (110) were made using a line-of-sight differentially pumped mass spectrometer shown in Figure 1. The crystal is mounted on a Ta plate (10 mm × 10 mm × 1 mm) using Ta clips which fit into slots machined on the crystal edges. A type K thermocouple is cemented into the interior corner of the crystal using Aremco type 571 cement. By using a digital temperature controller, the crystal temperature may be controlled accurately by ohmic heating of the assembly through tungsten wires welded to the back of the tantalum support plate. The crystal may be irradiated with selected wavelength regions of ultraviolet light of known flux incident at a 60° angle from the

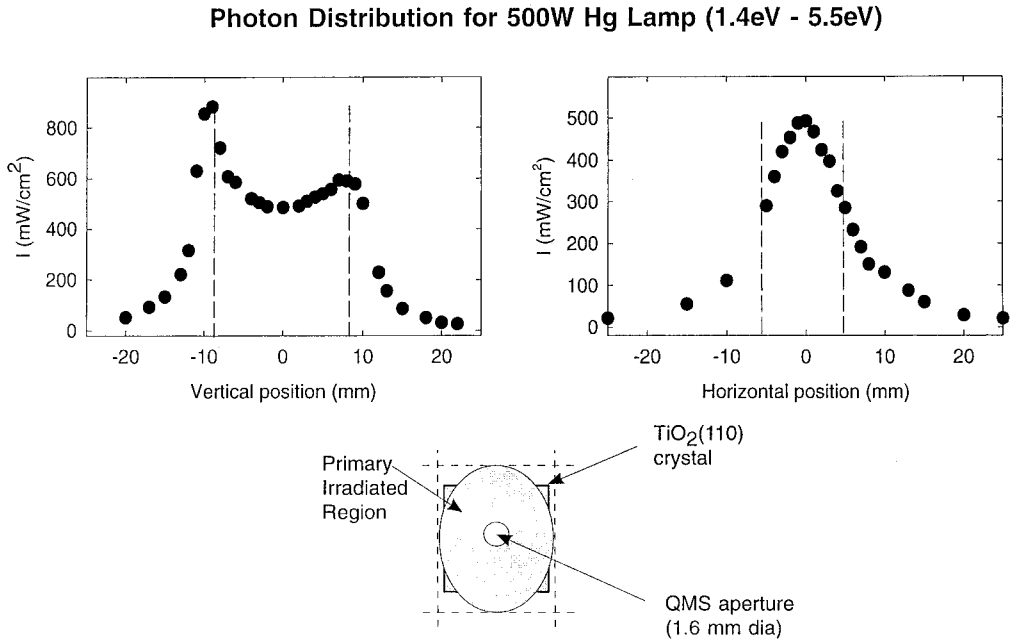

Figure 3. Photon distribution on the vertical and horizontal dimensions for a 500 W Hg lamp. The uniformly irradiated area of the TiO_2(110) crystal compared to the QMS aperture is schematically represented in the lower part of the figure.

normal to the crystal. Photodesorbing molecules are investigated using the differentially pumped mass spectrometer which samples the desorbing flux distribution centered in the normal direction through a 0.16 cm diameter aperture located 0.4 cm from the crystal surface.

Figure 2 shows the ultrahigh vacuum system used in these measurements. The crystal may be moved to various positions in the chamber for ion bombardment, Auger spectroscopy, and crystal dosing through an absolutely calibrated molecular beam doser,[27] which is not shown. The radiation from the 350 W mercury ultraviolet lamp source is filtered with a 10 cm column of distilled water to remove infrared radiation and then passes through an iris and focusing lenses. A narrow band-pass filter is inserted in the optical path as shown. By using a quartz beam splitter, 10% of the ultraviolet light is monitored during irradiation by a photodiode which has been cross-calibrated against a thermopile detector. For (3.96 ± 0.07) eV radiation, the incident flux on the crystal is 6.3×10^{14} photons/s cm^2. Figure 3 shows the distribution of lamp energy as a function of position in the focused beam of radiation from a 500 W lamp which behaves similarly to the 350 W lamp employed in this research. It may be seen that a fairly uniform distribution of light intensity occurs over the central 5 mm section of the distribution curves which have been measured in the vertical and horizontal direction, as shown in the profiles in the two top plots. In the bottom part of Figure 3, a schematic representation of the uniformly irradiated region on the crystal, compared to the mass spectrometer aperture, is shown.

The TiO_2 (110) crystal was prepared according to methods developed previously in this laboratory to produce a controlled coverage of O anion surface vacancies.[11] The crystal was initially bombarded with Ar^+ ions to remove carbonaceous impurities present after handling in the laboratory air. The subsequent chemical preparation procedure involves oxidation of the crystal by annealing at 900 K in an O_2 flux (1.1×10^{13} molecules/s cm^2) momentarily, followed by cooling at −0.8 K/s to 300 K in the same O_2 flux supplied by the molecular beam doser for 4 h. The crystal was then activated by heating momentarily at 900 K in ultrahigh vacuum. Approximately 10% of the surface is defective after this treatment.[11]

Isotopically labeled ^{15}NO was obtained from Cambridge Isotope Laboratories, and was purified by freeze−pump−thaw cycles. The isotopic purity was 99.0% ^{15}N.

It was of interest to evaluate the relative quantum efficiency for the photoproduction of $^{15}N_2O$(g) and ^{15}NO(g) in these experiments. The mass spectrometer was carefully calibrated against known pressures of $^{15}N_2O$ and ^{15}NO, using the ionization gauge in the main vacuum system, calibrated carefully for its sensitivity to each gas. Here, for the ionization gauge calibration, the sensitivities of the gases normalized to Ar were determined by using the molecular beam doser to supply gas at a known flow rate to the pumped vacuum system. The sensitivities are $S_g(^{15}N_2O) = 0.98$ and $S_g(^{15}NO) = 0.57$ relative to Ar[S_g(Ar) = 1.00]. The measured sensitivity of the mass spectrometer was determined as $S_{ms}(^{15}N_2O\text{-}46\ \text{amu}) = 12.1$ A/Torr, and $S_{ms}(^{15}NO\text{-}31\ \text{amu}) = 3.8$ A/Torr using an electron emission current of 2.00 mA at 70 eV ionization energy.

B. NO Photochemistry on Powdered TiO_2. In addition to the study of the photochemistry of adsorbed NO on the TiO_2 (110) surface, we have also studied the same photochemistry on powdered TiO_2 using transmission infrared spectroscopy. The powdered TiO_2 (Degussa ~50m^2/g surface area) is hydraulically pressed at 30 000 lbs/in^2 into a photoetched tungsten foil grid of 0.0051 cm thickness. This grid contains thousands of 0.22 mm × 0.22 mm windows filled with the compressed TiO_2 powder. The grid is supported inside an infrared cell using Ni clamps along the grid edges. Through cryogenic cooling and electronically controlled ohmic heating of the grid, one can program the TiO_2 temperature from 110 K to above 1500 K, and can electrically maintain constant temperature in this range with an accuracy of ±1 K. The grid is mounted in the cell at a 45° angle to the IR beam, so that irradiation of the grid with ultraviolet light directed perpendicularly to the IR beam can be carried out without making a geometrical change. A side view and top view of this apparatus are shown in Figure 4, and the sample pressing technique and the operation of the dual beam cell is described in ref 28. The UV source is a 350 W Hg lamp (Oriel Corp.; ref 29) with a 350 ± 50 nm band-pass filter. The photon flux at 350 nm is 1.7×10^{15} photons cm^{-2} s^{-1}.

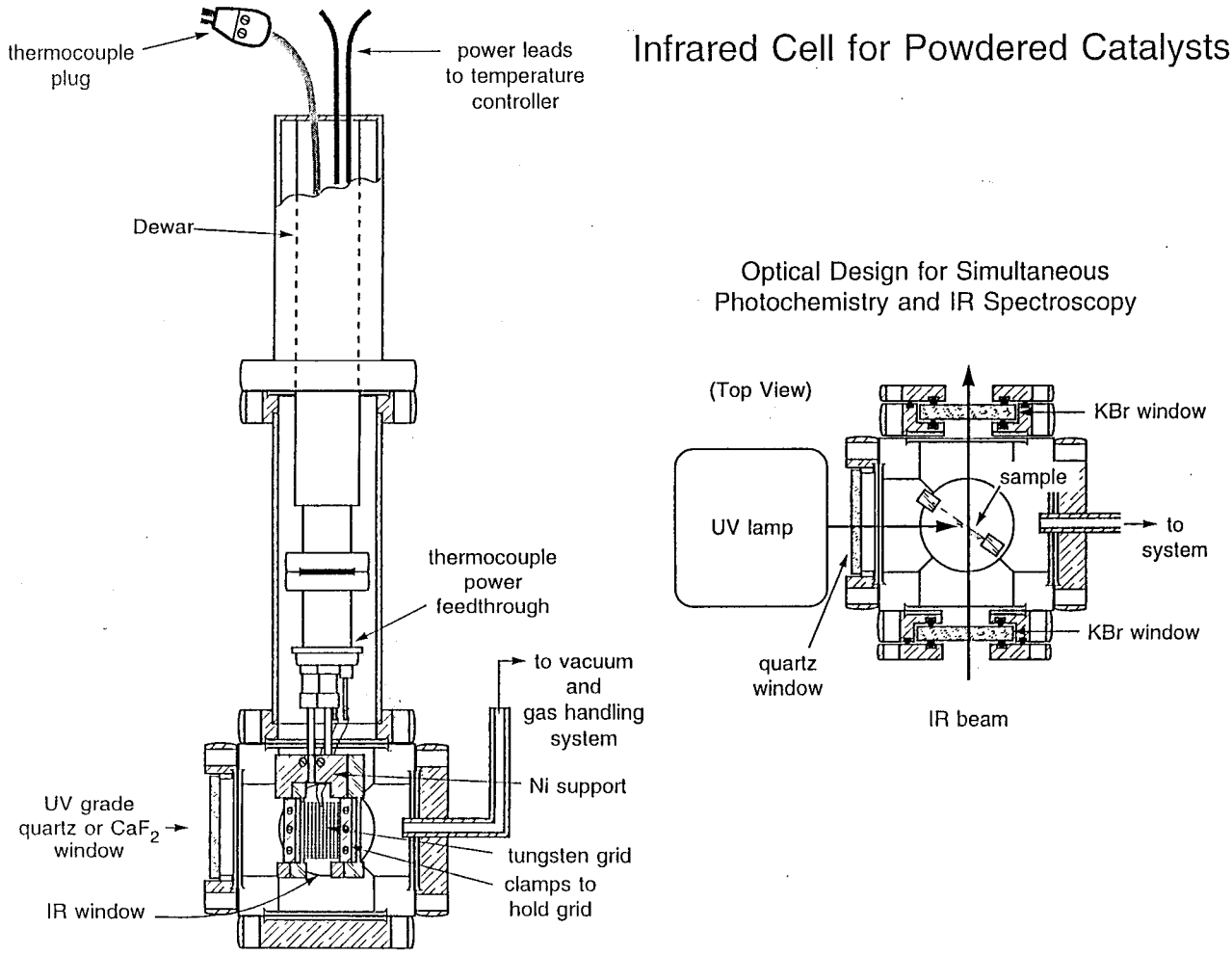

Figure 4. IR cell for studies on TiO_2 powder. The optical arrangement for simultaneous photochemistry and IR spectroscopy studies is shown.

III. Experimental Results

A. Studies on TiO_2(110). Figure 5 shows the primary result obtained when ^{15}NO (NO exposure = 2.2×10^{14} molec/cm^2) is irradiated with 3.96 eV ultraviolet radiation. Immediately upon opening the shutter to the light source, a pulse of $^{15}N_2O$ (m/e = 46) photoproduct is observed, and a decay of the $^{15}N_2O$ desorption rate occurs. The decay may be fitted by a double exponential decay rate law as indicated by the excellent fit to a pair of exponential curves. N_2O is a major photochemical decomposition product of adsorbed NO on TiO_2 (110).

Figure 6 shows the behavior of the (m/e = 31) photodesorption product obtained by multiplexing the mass spectrometer between (m/e = 46) and (m/e = 31) during the same experiment as shown in Figure 5. The majority of the (m/e = 31) signal in Figure 5 originates from the $^{15}NO^+$ cracking product of the $^{15}N_2O$ photoproduct. However, the behavior of the (m/e = 31) desorption curve differs from that seen for the (m/e = 46) curve since the exponential curves describing the $^{15}N_2O$ photoproduction deviate from the experimental measurement at (m/e = 31). This difference is shown by the crosshatched region in the top panel of Figure 6. This crosshatched region represents an additional photodesorption signal that originates as a result of the simultaneous photodesorption of ^{15}NO which also yields an (m/e = 31) ion. We have measured in separate experiments that the mass spectrometer cracking pattern for pure $^{15}N_2O$ produces an ion yield ratio (m/e = 31)/(m/e = 46) = (0.70 ± 0.05) for 70 eV electron impact ionization in the QMS, and this cracking pattern ratio has been used to make the comparison shown in the top panel of Figure 6.

The photodesorption of ^{15}NO from TiO_2 (110) may be measured from the difference between the experimental data in the top panel of Figure 6 and the calculated contribution of $^{15}N_2O$ to this signal at (m/e = 31), and this difference is shown in the bottom panel of Figure 6. This difference represents the photodesorption behavior for ^{15}NO(a). The photodesorption rate for ^{15}NO is very small at the beginning of the photolysis experiment, grows to a maximum after about 60 s of irradiation, and then decreases to zero over a period of about 300 s. It is clear that changes on the surface which occur during irradiation of chemisorbed ^{15}NO cause the desorption yield of ^{15}NO to increase and then to decrease.

It was of interest to calculate an average integral photoyield of N_2O and NO from these data. In Figure 7, the photoinduced production of $^{15}N_2O$ and ^{15}NO are shown using the same time scale as abscissa. In the top panel, the integrated yield of $^{15}N_2O$ over a time period of 2 s was evaluated when the surface received 1.2×10^{15} photons/cm^2. In the bottom panel of Figure 7 the average integral photoyield of ^{15}NO was similarly calculated over a 300 s time period where 1.8×10^{17} photons/cm^2 were received by the crystal. These results will be employed in the Discussion of the results.

Preliminary studies of the influence of various photon energies on the photoproduction of N_2O(g) were made as shown in Figure 8, for photon energies from 1.8 to 3.96 eV. These results prove that a relatively low efficiency excitation involving sub-bandgap

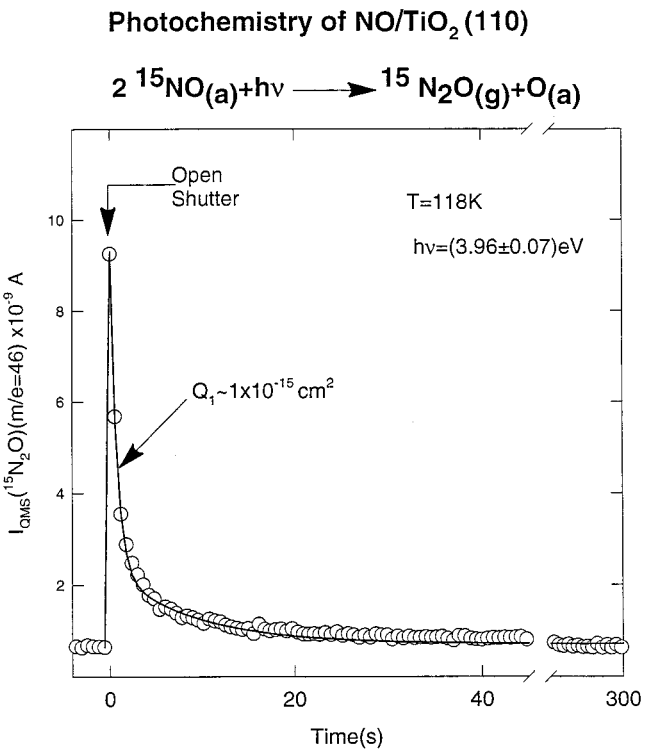

Figure 5. $^{15}N_2O$ photoproduced on TiO_2(110). The desorption curve is best fitted (continuous line) to a sum of two exponential curves, giving the cross sections $Q_1 = 1 \times 10^{-15}$ cm^2 and $Q_2 = 8 \times 10^{-17}$ cm^2.

photon energy occurs. For a photon energy of 2.3 eV, N_2O(g) is photoformed on the defective surface, but the yield per photon is comparatively small. Experiments conducted using 1.8 eV photons showed very small amounts of N_2O(g) were photoformed. Our studies of the UV transmission spectra of the UV filters used indicate that the results of Figure 8 cannot be attributed to a low level transmission of radiation with energy of 3.2 eV (or more) for the longer wavelength filters used.

B. Studies on Powdered TiO_2. The adsorption of ^{14}NO on the powdered TiO_2 sample was carried out after oxidation of the TiO_2 at 673 K in O_2 (g) at 50 Torr, followed by activation of the surface by heating in a vacuum to 673 K for 13 h to produce anion vacancy defect sites necessary for the adsorption of ^{14}NO.

The development of the infrared spectra for the adsorbed ^{14}NO as a function of exposure at 110 K is shown in Figure 9. Modes at 1724, 1741, 1837, 1869, 1898, 1920, 2237, and 2258 cm^{-1}, respectively, are observed to develop as ^{14}NO adsorption proceeds. Modes at 1724, 1741, 1837, 1869, 1898, and 1920 cm^{-1}are assigned to the $^{14}N-O$ stretching mode for various ^{14}NO species bound at different sites on the polycrystalline TiO_2 surface. Modes at 2237 and 2258 cm $^{-1}$ are assigned to the $^{14}N-^{14}N$ stretching mode for $^{14}N_2O$ produced on the TiO_2 surface by ^{14}NO adsorption at 110 K. Infrared spectroscopic studies of ^{15}NO adsorption support these assignments.

Figure 10 shows the effect of ultraviolet irradiation on the ^{14}NO-covered surface. ^{14}NO modes characteristic of chemisorbed ^{14}NO decrease in absorbance, while modes associated with adsorbed $^{14}N_2O$ species increase in absorbance. The modes at 2258 and 2237 cm^{-1} are assigned to the ν(NN stretch) from $^{14}N_2O$ adsorbed on TiO_2. The modes at 1311, 1255, and 1162 cm^{-1} are assigned to ν(NO stretch) from $^{14}N_2O$ adsorbed on TiO_2. $^{14}N_2O$ adsorption experiments on TiO_2 powder were carried out independently and proved that modes at 2258, 2237,

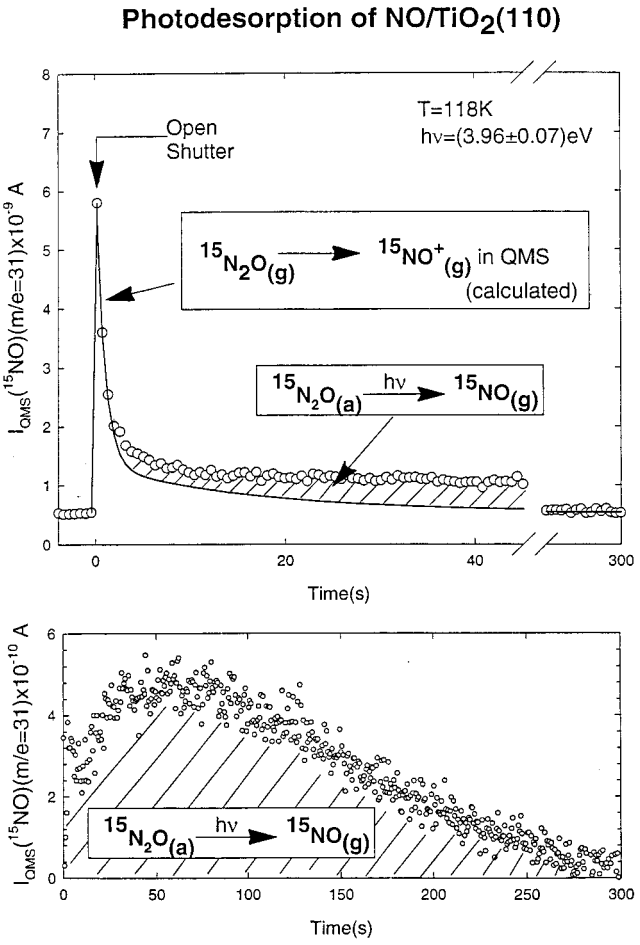

Figure 6. ^{15}NO photodesorption from TiO_2(110). In the upper panel is shown the decay of the ($m/e = 31$) signal with time. The continuous line corresponds to the $^{15}NO^+$ cracking pattern of the photoproduced $^{15}N_2O$. The crosshatched area shows the $^{15}NO^+$ signal which cannot be explained by the mass spectrometer cracking of $^{15}N_2O$. The lower panel shows the ^{15}NO evolution with time during irradiation (see text).

1311, 1255, and 1162 cm^{-1} are associated with N_2O adsorbed on TiO_2. The production of N_2O on the powdered TiO_2 surface is in agreement with the measurements presented earlier for the same photoreaction on TiO_2(110). Upon warming the powdered TiO_2 to 300 K after exposure to UV radiation, N_2O(g) was liberated and the N_2O(g) spectrum was observed by transmission infrared spectroscopy through a portion of the grid which does not contain TiO_2.

Figure 11 shows the development of the relative integrated absorbance from chemisorbed NO and chemisorbed N_2O during the photochemical decomposition of adsorbed NO at 110 K. The relative integrated absorbance was obtained from the integrated absorbance after a specific time of irradiation ratioed to the integrated absorbance before irradiation. A monotonic decrease in the integrated absorbance of NO is observed, combined with a monotonic increase in the absorbance of the N_2O photoproduct adsorbed on the TiO_2 powder. After extensive photolysis of the NO, the TiO_2 sample was heated for 30 min to 124 K and cooled back to 110 K, and then the photolysis was continued at 110 K. It is seen that the *rate of change* of the N_2O and NO infrared absorbances is almost not influenced by the 124 K annealing process, although an absorbance discontinuity is observed upon this heat treatment.

Two features in Figure 11 are noteworthy. First, upon ultraviolet irradiation, the chemisorbed NO is extensively converted to N_2O, judging from the large fractional decrease

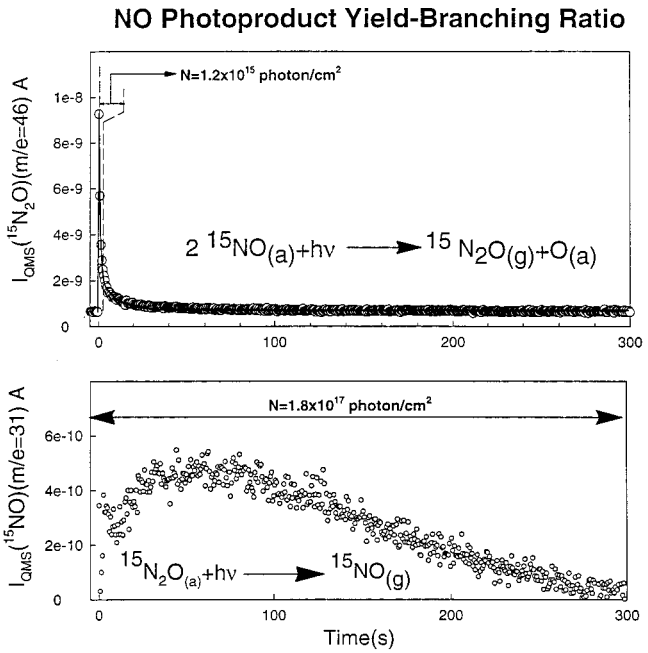

Figure 7. The evolution of the photoproduced $^{15}N_2O$ and of the photodesorbed ^{15}NO. The photon fluences over time periods corresponding approximately to N_2O and NO production are shown.

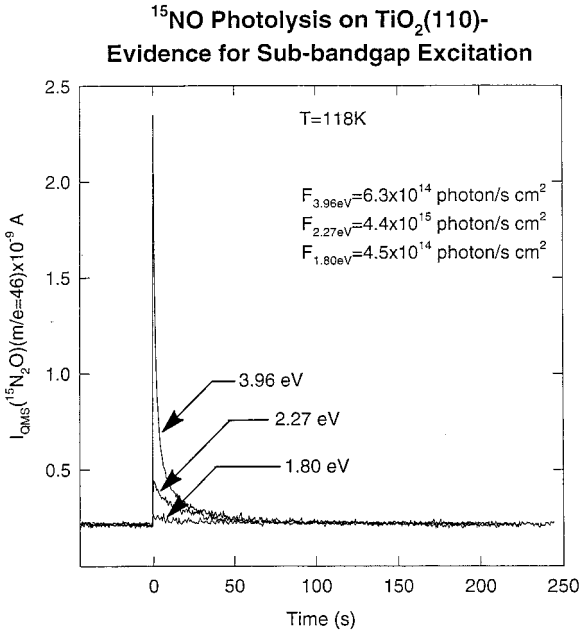

Figure 8. NO photolysis on TiO_2(110)-evidence for sub-bandgap excitation. The dependence of the $^{15}N_2O$ photodesorption on photon energy.

in the NO integrated absorbance accompanied by a large fractional increase in the adsorbed N_2O integrated absorbance. Second, annealing after extensive photolysis does not produce a surface condition where the rate of photochemical consumption of NO is significantly enhanced, or the rate of production of chemisorbed N_2O product is significantly enhanced. This annealing experiment therefore strongly suggests that the extensive consumption of adsorbed NO during irradiation is not influenced by thermally activated surface diffusion of NO from the interior regions of the compressed powder to the surface region. Instead, penetration of ultraviolet irradiation far into the depth of the powdered TiO_2 sample occurs, causing NO photodecomposition deep in the interior of the pressed TiO_2 sample.

IV. Discussion

A. The Photochemical Efficiency of Decomposition of Chemisorbed NO. Figure 5 shows the production of $^{15}N_2O$ from the photochemical decomposition of ^{15}NO on the TiO_2 (110) crystal. We assume that the photochemical mechanism may be represented by two elementary steps, shown below,

$$\mathrm{NO(a)} + h\nu = \mathrm{N^*(a)} + \mathrm{O(a)} \quad [Q_1 \text{ is cross section}] \quad (1)$$

$$\mathrm{N^*(a)} + \mathrm{NO(a)} = \mathrm{N_2O(g)} \quad [k_2 \text{ is rate constant}] \quad (2)$$

The symbol N* represents an excited nitrogen atom, where the excitation of N*, achieved by the primary photodissociation event, is in the form of excess translational energy. Assuming the steady-state approximation for the two reactions, we can write

$$-\mathrm{d}\Theta_{\mathrm{NO}}/\mathrm{d}t = 2Q_1\Theta_{\mathrm{NO}}F_{h\nu} \quad (3)$$

where $F_{h\nu}$ is the flux of 3.96 eV photons onto the surface and Θ_{NO} is the NO surface coverage.

The most rapid exponential decay rate of the N_2O signal during photochemical depletion of NO may be used to determine Q_1, the cross section for the primary excitation reaction, and this value for (3.96 ± 0.07) eV photons is $Q_1 = 1 \times 10^{-15}$ cm^2, as shown by the fit in Figure 5.

Figures 5 and 6 show that N_2O(g) is initially produced rapidly by the photochemical decomposition of adsorbed NO. During the later stages of N_2O(g) production, an NO desorption process becomes active, maximizes its rate, and then decreases in magnitude. For the purpose of approximately characterizing the relative and absolute quantum yields of the two processes, we have adopted an integral measurement method. Figure 7 shows the two processes plotted on the same time scale, and the number of photons/cm^2 associated with somewhat arbitrary integrations over the two processes.

The relative quantum yield for N_2O production and for NO desorption, evaluated integrally over the time periods shown is

$$\text{relative quantum yield} = \frac{Y^{\text{photodesorbed}}_{\mathrm{NO}\rightarrow 1/2\mathrm{N_2O_{(g)}}}/\text{photon}}{Y^{\text{photodesorbed}}_{\mathrm{NO_{(g)}}}/\text{photon}} \cong 12 \quad (4)$$

The absolute quantum yields, evaluated integrally, is

$$[Y^{\text{photodesorbed}}_{\mathrm{NO}\rightarrow 1/2\mathrm{N_2O_{(g)}}}/\text{photon}] \cong 0.7\% \quad (5)$$

$$[Y^{\text{photodesorbed}}_{\mathrm{NO_{(g)}}}/\text{photon}] \cong 0.06\% \quad (6)$$

The absolute yield of the two photoproducts per joule of incident 3.96 eV photons, evaluated integrally is

$$[Y^{\text{photodesorbed}}_{\mathrm{NO}\rightarrow 1/2\mathrm{N_2O_{(g)}}}/\mathrm{W\ s}] \cong 1.1 \times 10^{16}\ \text{molec/J} \quad (7)$$

$$[Y^{\text{photodesorbed}}_{\mathrm{NO_{(g)}}}/\mathrm{W\ s}] \cong 9.2 \times 10^{14}\ \text{molec/J} \quad (8)$$

The measurements of the initial rate of NO depletion, evaluated from the cross section for the change of the rate of N_2O production at a known photon flux, allows one to make a comparison to the mass spectrometric integral yields of N_2O(g) and NO(g). The NO depletion cross section of $\sim 1 \times 10^{-15}$ cm^2 corresponds to a quantum efficiency near unity. The quantum yields of N_2O(g) and NO(g), in the range $10^{-2}-10^{-4}$, indicate that the photodesorption measurement witnesses only minor

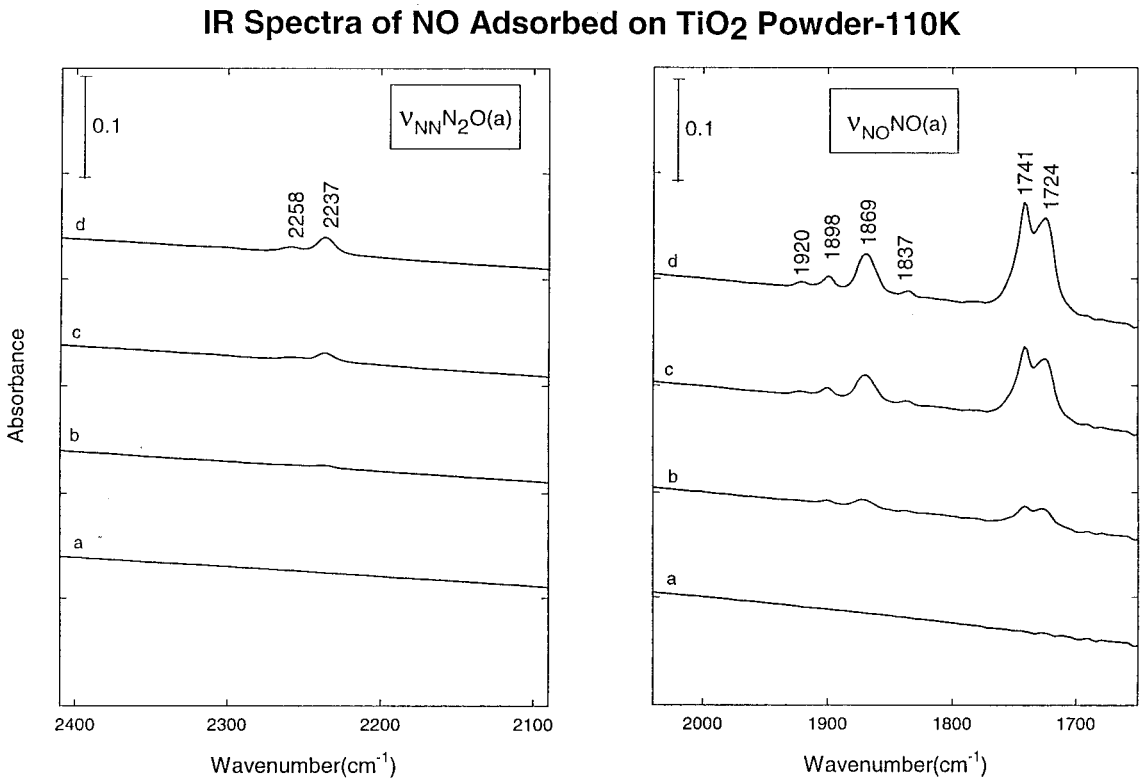

Figure 9. IR spectra of the adsorbed NO on TiO_2 powder as a function of NO exposure at 110 K: (a) no NO added; (b) 3.84×10^{17} NO molecules added; (c) 9.7×10^{17} NO molecules added; (d) 1.69×10^{18} NO molecules added.

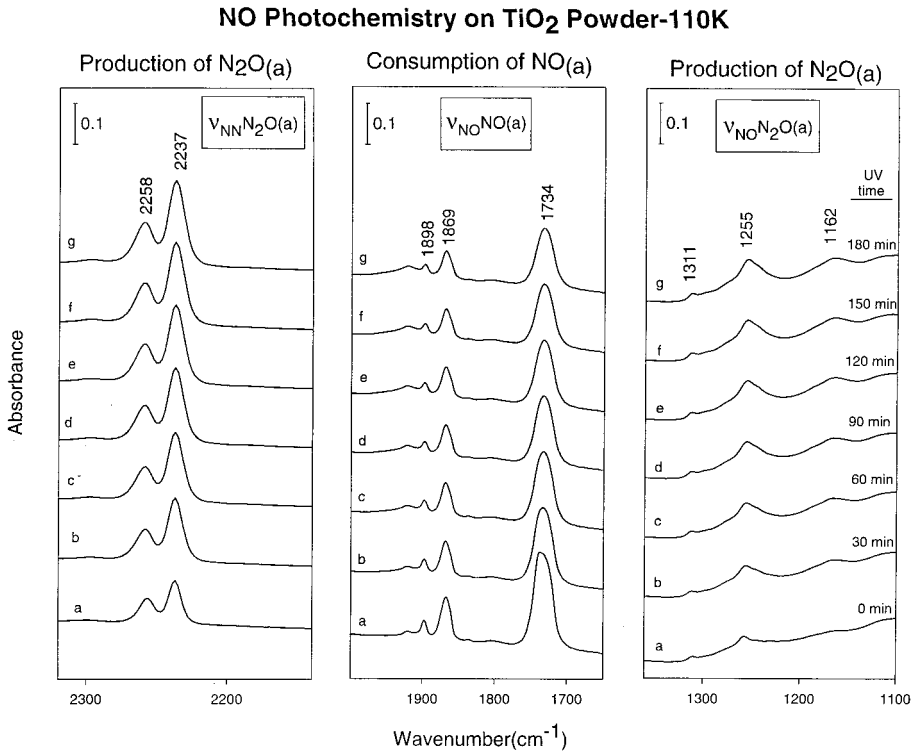

Figure 10. NO photochemistry on TiO_2 powder at 110 K. IR spectra in the region of ν(NN) and ν(NO) for N_2O produced from NO on TiO_2 powder (left and right panels) and IR spectra in the region of ν(NO) for NO adsorbed on TiO_2 powder (middle panel). The number of NO molecules added to the TiO_2 sample prior to irradiation was 1.1×10^{19} NO molecules.

photochemical processes compared to the major process causing NO depletion. We postulate that the major process is the capture of a photoproduct by the TiO_2(110) surface. This is probably chemisorbed N_2O, which has been observed in two different experiments:[1] on TiO_2(110), TPD after photodecomposition of NO shows that N_2O is evolved;[2] on powdered TiO_2, chemisorbed N_2O is observed to form during NO photolysis (Figure 11).

These photochemical efficiency measurements allow one to approximately estimate the engineering efficiency of an NO

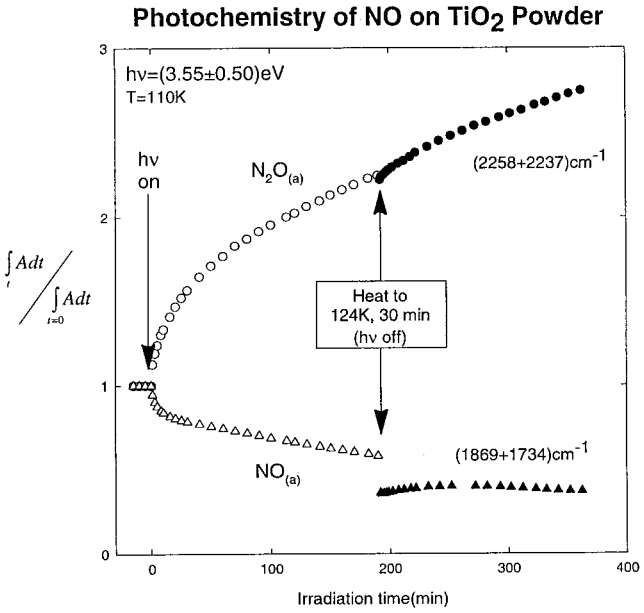

Figure 11. NO photochemistry on TiO_2 powder at 110 K: Kinetics plots for the consumption of NO and the production of N_2O. An annealing experiment at 124 K is shown after considerable photodepletion of chemisorbed NO to test the hypothesis that NO diffusion from deep within the compressed powder supplies NO to a ~200 Å thick outer surface layer of the powder for photoactivation. The hypothesis is not supported by this experiment.

photoreactor for use in the photodecomposition of NO by ultraviolet excitation of chemisorbed NO.

B. The Mechanism of NO Photochemistry on TiO_2. It is believed that electron−hole pair excitation within the near surface region of TiO_2 is responsible for the photoexcitation of adsorbed molecules.[20] For photoactive O_2 molecules on TiO_2 surfaces, a photon excitation threshold energy near the band gap energy, $E_{gap} = 3.2$ eV, is found for both the photodesorption of molecular O_2[29−32] and for surface photochemical reactions caused by the excitation of adsorbed O_2.[12,13] While it has not been proven that this excitation is due to electron attachment to the adsorbed O_2 molecule, this has been assumed in a number of studies.[20]

For NO photoexcitation on TiO_2, we assume that band gap excitation of electron−hole pairs is also responsible for excitation of the NO. However, as shown in Figure 8, there is evidence that photon energies less than 3.2 eV are also slightly effective in causing the photochemical production of N_2O from chemisorbed NO.

Two explanations for the sub-bandgap excitation may be considered.

(1) Direct electron excitation from the solid to an unoccupied molecular orbital present in the band gap energy region may also play a role in the photoexcitation of the chemisorbed NO molecule. The first such empty state lies approximately 6 eV above the ground state for NO(g).[33] The production of N* species, which react with neighbor NO molecules is postulated on the basis of the production of N_2O, as shown in eq 1, but other mechanisms for N_2O production involving excited NO species on the surface may also be imagined.

(2) The excitation process for photon energies lower than the band gap may be correlated with the existence of the electronic states in the band gap of the reduced semiconductors. Such a subgap excitation process was seen for example from measurements of photoconductivity of ZnO.[34] These electronic states are generated in the process of defect site creation. For TiO_2 (110) the electronic states associated with the defect sites are located around 0.7 eV below the conduction band edge.[35−37]

The curious lack of NO photodesorption at the beginning of the photochemical reaction, followed by a gradual increase in the yield of photodesorbing NO as the irradiation proceeds, is not currently understood.

We postulate that the slow rate of increase in the NO photodesorption rate may be related to the capture of photoproduced N_2O by the surface and its slow subsequent photodecomposition to NO(g). Experiments with adsorbed N_2O will be employed to check this hypothesis.

C. NO Photochemistry on TiO_2 Powder. The studies of NO photochemistry on TiO_2 (110) at 118 K provide a quantitative basis for estimating the efficiency of the basic photochemical processes involved in NO activation. However, practical schemes using powdered TiO_2 surfaces for NO photochemistry will also be governed by issues such as adsorbate contact time with the TiO_2, depth of photochemical excitation within the powdered TiO_2 layer, transport rate of NO through the depth of the powdered bed, and the chemical nature of the adsorbed NO molecules as a function of the surface temperature.

It is well appreciated that the depth of penetration of ultraviolet radiation into a solid TiO_2 crystal is very small. For polycrystalline rutile at 326 nm (3.80 eV), the absorption coefficient is 5×10^5 cm^{-1}.[38] This corresponds to a photon attenuation length of only 200 Å. Thus, if a thick powdered TiO_2 sample were to limit photon access to only the first few hundred angstroms of depth, only a small fraction of the adsorbate would be able to be photolyzed. For the infrared photolysis studies shown in Figures 9−11, involving pressed TiO_2 powder samples of a thickness of 5×10^{-3} cm, the strong attenuation expected in the first 200 Å thickness would allow only a tiny fraction (approximately 4×10^{-4}) of the adsorbed NO to be photolyzed. In contradiction to this expectation, the experiments shown in Figures 10 and 11 for the photolysis of NO clearly indicate that approximately one-half of the adsorbed NO can be photolyzed on the powdered TiO_2 deposits in the time period used in the experiments.

There are two explanations which may be offered to explain the large photochemical depletion depth in the powdered samples.

(1) Photochemistry occurs only at penetration depths of the order of hundreds of angstroms, and NO diffusion from deeper levels via surface diffusion and particle-to-particle transport processes occurs to refill the outer surface sites.

(2) Ultraviolet light penetrates deeply into the powder samples as a result of light transport along the interfaces between the packed particles in the deposit.

The experiment shown in Figure 11 suggests that explanation 2 is correct. In Figure 11, the photodissociation of a significant fraction of the adsorbed NO is carried out at 110 K, and then the sample is warmed briefly to 124 K to allow particle-to-particle diffusion of NO to refill the outer region of the packed powder deposit. This should result in a dramatic increase in the rate of photodepletion of the NO as observed by IR spectroscopy, since NO from the depth of the sample would repopulate the surface region of the powder where photons are available. Such an effect was not found, and instead, the kinetics of NO depletion and N_2O production were hardly affected by the heating experiment.

Therefore, it is suggested that even though the attenuation length for the ultraviolet light in a single crystal of TiO_2 is only about 200 Å, ultraviolet light scattering through compressed powder deposits of TiO_2 occurs to depths which are of the order

of at least 0.003 cm, i.e., approximately through one-half of the physical thickness of the powdered samples employed here. The effective depth for photochemical activation in compressed TiO_2 powders far exceeds the ultraviolet attenuation length in individual crystals of TiO_2.

V. Summary of Results

The photochemical decomposition of chemisorbed NO on TiO_2 surfaces has been studied using both single-crystal TiO_2 (110) and powdered high area TiO_2 substrates.

The following results have been obtained.

(1) N_2O is a primary desorption product, and at photon energies of 3.96 eV, this molecule is rapidly produced and desorbed from TiO_2 (110). Infrared studies on powdered TiO_2 show that N_2O is also photoproduced.

(2) The cross section for the rapid photodepletion of chemisorbed NO on TiO_2 (110) is 1×10^{-15} cm^2, and this NO depletion process controls the rate of gas-phase N_2O production. The quantum yield for NO photodepletion corrresponding to this cross section is approximately unity. Quantitative measurements of the N_2O production indicate that the integral quantum yield of NO conversion to gas-phase N_2O is about 0.7×10^{-2} NO/photon at 3.96 eV.

(3) A slow photoproduction of gas-phase NO is observed following extensive NO depletion. The integral quantum yield for this process is about 6×10^{-4} NO/photon at 3.96 eV.

(4) The comparison between the high cross section for adsorbed NO depletion and the small quantum yields for N_2O(g) and NO(g) photoproduction indicates that the dominant photoprocess is the photochemical conversion of adsorbed NO to adsorbed N_2O.

(5) The photodecomposition of chemisorbed NO occurs at depths of the order of 0.003 cm in compressed TiO_2 powder. This depth far exceeds the known attenuation length of ultraviolet light in single crystals of TiO_2 (about 200 Å), indicating that ultraviolet light can penetrate deeply into TiO_2 powders by light transport effects at the powder grain boundaries, greatly enhancing the efficiency of the surface photochemistry.

(6) Evidence for the photoproduction of N_2O from chemisorbed NO on TiO_2 at photon energies below the 3.2 eV TiO_2 band gap has been found; even at 1.8 eV, a very low efficiency of N_2O production is observed. This effect may be due to electronic excitations from defect-related filled electronic states in the band gap region.

Acknowledgment. We thank the Army Research Office for support of this work.

References and Notes

(1) Busca, G.; Lietti, L.; Ramis, G.; Berti, F. *Appl. Catal. B: Environmental* **1998**, *18*, 1.

(2) Hashimoto, K.; Fukuhara, K.; Fujiwara, Y.; Kominami, H.; Mishima, H.; Kera, Y. *Appl. Catal. A: General* **1997**, *165*, 451.

(3) Haneda, M.; Kintaichi, Y.; Inaba, M.; Hamada, H. *Catal. Today* **1998**, *42*, 127.

(4) Zhang, S.; Kobayashi, T.; Nosaka, Y.; Fujii, N. *J. Mol. Catal. A: Chem.* **1996**, *106*, 119.

(5) Iwamoto, M.; Yahiro, H.; Shundo, S.; Yu-U, Y.; Mizuno, N. *Appl. Catal.* **1991**, *69*, L15.

(6) Kintaichi, Y.; Hamada, H.; Tabata, M.; Sasaki, M.; Ito, T. *Catal. Lett.* **1990**, *6*, 239.

(7) Hamada, H.; Kintaichi, Y.; Sasaki, M.; Ito, T.; Tabata, M. *Appl. Catal.* **1991**, *75*, L1.

(8) Miyadera, T. *Appl. Catal.* **1993**, *B2*, 199.

(9) Rives-Arnau, V.; Munuera, G. *Appl. Surf. Sci.* **1980**, *6*, 122.

(10) Yang, R. T.; Li, W. B.; Chen, N. *Appl. Catal. A: General* **1998**, *169*, 215.

(11) Lu, G.; Linsebigler, A.; Yates, J. T., Jr. *J. Chem. Phys.* **1994**, *98*, 11733.

(12) Linsebigler, A.; Lu, G.; Yates, J. T., Jr. *J. Chem. Phys.* **1995**, *103*, 9438.

(13) Linsebigler, A.; Lu, G.; Yates, J. T., Jr. *J. Chem. Phys.* **1996**, *100*, 6631.

(14) Boccuzzi, F.; Guglielminotti, E.; Spoto, G. *Surf. Sci.* **1991**, *251/252*, 1069.

(15) Boccuzzi, F.; Guglielminotti, E.; Chiorino, A. *Sens. Actuators* **1992**, *B7*, 645.

(16) Boccuzzi, F.; Guglielminotti, E. *Sens. Actuators* **1994**, *B21*, 27.

(17) Guglielminotti, E.; Boccuzzi, F. *J. Chem. Soc., Faraday Trans.* **1991**, *87* (2), 337.

(18) Pande, N. K.; Bell, A. T. *J. Catal.* **1986**, *97*, 137.

(19) Dines, T. J.; Rochester, C. H.; Ward, A. M. *J. Chem. Soc., Faraday Trans.* **1991**, *87* (4), 643.

(20) Linsebigler, A.; Lu, G.; Yates, J. T., Jr. *Chem. Rev.* **1995**, *95*, 735.

(21) Dai, H.-L.; Ho, W. *Laser spectroscopy and photochemistry on metal surfaces*; World Scientific: River Edge, NJ, 1995; Part II.

(22) Pichat, P.; Herrmann, J.-M.; Courbon, H.; Disdier, J.; Mozzanega, M. N. *Can. J. Chem. Eng.* **1982**, *60*, 27.

(23) Courbon, H.; Pichat, P. *J. Chem. Soc., Faraday Trans. 1* **1984**, *80*, 3175.

(24) Ibusuki, T.; Takeuchi, K. *J. Mol. Catal.* **1994**, *88*, 93.

(25) Schaper, K.; Hesse, D. *Chem.-Ing.-Tech.* **1994**, *66* (1), 86.

(26) Yamashita, H.; Ichihashi, Y.; Anpo, M.; Hashimoto, M.; Louis, C.; Che, M. *J. Phys. Chem.* **1996**, *100/40*, 16041.

(27) Winkler, A.; Yates, J. T., Jr. *J. Vac. Sci. Technol.* **1988**, *A6*, 2929.

(28) Ballinger, T. H.; Wong, J. C. S.; Yates, J. T., Jr. *Langmuir* **1992**, *8*, 1676.

(29) *29.Light sources, Monochromators, Detection Systems*; Oriel Corporation, Oriel Catalog; p 82.

(30) Lu, G.; Linsebigler, A.; Yates, J. T., Jr. *J. Chem. Phys.* **1995**, *102*, 3005.

(31) Lu, G.; Linsebigler, A.; Yates, J. T., Jr. *J. Chem. Phys.* **1995**, *102*, 4657.

(32) Rusu, C. N.; Yates, J. T., Jr. *Langmuir* **1997**, *13*, 4311.

(33) G. Herzberg, G. *Spectra of Diatomic Molecules*; Van Nostrand Reinhold Company: New York, 1950; p 422.

(34) Schindler, K.-M.; Kunst, M. *Chem. Phys. Lett.* **1990**, *172*, 137 and references therein.

(35) Munnix, S.; Schmeits, M. *Phys. Rev. B* **1985**, *31*, 3369.

(36) Henrich, V. E.; Dresselhaus, G.; Zeiger, H. F. *Phys. Rev. Lett.* **1976**, *36*, 1355.

(37) Chung, W.; Lo, W. J.; Somorjai, G. A. *Surf. Sci.* **1977**, *64*, 588.

(38) Cronemeyer, D. C. *Phys. Rev.* **1952**, *87*, 876.